RESEARCH ARTICLE

NANO · MICRO small
www.small-journal.com

2D and 3D Micropatterning of Mussel-Inspired Functional Materials by Direct Laser Writing

*Zeynab Tavasolyzadeh, Peng Tang, Marc Benjamin Hahn, Gada Hweidi, Niclas Nordholt, Rainer Haag, Heinz Sturm, and Ievgeniia Topolniak**

This work addresses the critical need for multifunctional materials and substrate-independent high-precision surface modification techniques that are essential for advancing microdevices and sensing elements. To overcome existing limitations, the versatility of mussel-inspired materials (MIMs) is combined with state-of-the-art multiphoton direct laser writing (DLW) microfabrication. In this way, 2D and 3D MIM microstructures of complex designs are demonstrated with sub-micron to micron resolution and extensive post-functionalization capabilities. This study includes polydopamine (PDA), mussel-inspired linear, and dendritic polyglycerols (MI-lPG and MI-dPG), allowing their direct microstructure on the substrate of choice with the option to tailor the patterned topography and morphology in a controllable manner. The functionality potential of MIMs is demonstrated by successfully immobilizing and detecting single-stranded DNA on MIM micropattern and nanoarray surfaces. In addition, easy modification of MIM microstructure with silver nanoparticles without the need of any reducing agent is shown. The methodology developed here enables the integration of MIMs in advanced applications where precise surface functionalization is essential.

1. Introduction

Micropatterning techniques offer significant advantages for creating highly controlled spatially resolved substrates, which are especially required in integrated analytical devices, clinical diagnostics, environmental monitoring, and quality control. As we advance toward miniaturization, it has become necessary not only to develop simple and cost-effective microfabrication processes, but also to provide multifunctionality to the manufactured devices.

Various micro additive manufacturing techniques, including photolithography, microcontact printing, inkjet printing, digital light processing, micro laser sintering, and multiphoton direct laser writing (DLW), have been developed to achieve high-precision fabrication.[1] Contrasted with other methods, DLW stands up for its exceptional flexibility in 2D and 3D design, enabling for submicron/nanometer structural precision without the constraints imposed by the need for a layer-by-layer approach, micro-stamping/masking, or complicated multistep procedure.[2] This technique has promising potential in diverse fields, including sensing, biological, and tissue engineering.[3–5] Furthermore, this method facilitates the integration of microstructures into devices with curved surfaces, such as microfluidic chips and other MEMs. Coupled with the capability of multi-spot parallel processing[6,7] and the continued advances in increasing throughput, DLW holds significant potential for the further development of microdevice technology.

Nevertheless, even with the ability to precisely deposit fine 2D and 3D micro-architectures, it is often insufficient to deliver the required functionality. In addition to the functionality-by-design offered by DLW 3D freedom, the ability to efficiently functionalize the surface of choice plays a critical role in the successful deployment of the system. In addition, poor adhesion of the functional structure to the substrate is often a limiting factor in the selection of suitable materials.

To address these challenges, mussel-inspired materials (MIMs) have emerged as a substrate-independent universal coatings for tailoring the physical and chemical properties of nearly any surface of interest.[5] By mimicking the chemistry of mussel foot proteins, MIMs exhibit strong adhesion through covalent or non-covalent interfacial binding of the catechol moiety and present amines to a surface.[8–11] Moreover, capable of diverse chemical binding mechanisms, these coatings hold

Z. Tavasolyzadeh, M. B. Hahn, G. Hweidi, N. Nordholt, H. Sturm, I. Topolniak
BAM Bundesanstalt für Materialforschung und -prüfung
Unter den Eichen 87, 12205 Berlin, Germany
E-mail: ievgeniia.topolniak@bam.de
P. Tang, R. Haag
Institut für Chemie und Biochemie
Freie Universität Berlin
Takustrasse 3, 14195 Berlin, Germany
H. Sturm
TU Berlin
IWF
Pascalstr. 8–9, 10587 Berlin, Germany

The ORCID identification number(s) for the author(s) of this article can be found under https://doi.org/10.1002/smll.202309394

DOI: 10.1002/smll.202309394

high ability for a wide range of post-functionalization, ensuring the multifunctional versatility of their surface.

In this work, we aim to combine the microfabrication capabilities of DLW with the multifunctionality of MIM materials to create flexible by design and functional 2D and 3D microelements. Among the MIM materials, we selected dopamine and synthetically designed linear and dendritic polyglycerols (MI-lPG and MI-dPG, respectively) as they have shown great multifunctional capabilities. Polydopamine (PDA), due to its availability and low cost, has been used on the vast variety of materials as bio-adhesives, contrast agents, drug delivery systems, sensing et al.[12,13] Recently designed to mimic not only the functional groups but also their molecular weight and structure of mussel foot proteins,[14,15] MI-dPG has been shown to form a highly stable coating by simple dip-coating, regardless of the nature of the substrate, within a considerably short time. This MIM can be used as a micro-anchor for various functionalizations[16] and applied to create superhydrophobic,[14] antifouling, and bactericidal surfaces.[15,17]

Despite the great potential of MIMs, little work has been done to study the micropatterning of these versatile coatings. While no micropatterning has been reported for mussel-inspired polyglycerols (MI-PGs) yet, some has been performed for PDA using photolithography,[18] microcontact printing[19,20], or its combination with UV-initiated polymerization.[21,22] However, the microstamps and photomasks used for such approaches result in resolutions in the hundreds of microns, tens of microns at best, and often require tedious multi-step processes. Our first attempts at multiphoton DLW 2D patterning of dopamine showed the ability to trigger its polymerization in the presence of a suitable photoinitiator.[23] However, we faced the challenges in fabricating 3D structures and limitations in the fabrication throughput. Therefore, further research is needed to fully explore the potential of these versatile multifunctional materials for microfabrication.

In this study, we present high-precision 2D and 3D DLW microstructuring of mussel-inspired dendritic and linear polyglycerols and polydopamine as a platform for localized, highly precise, controllable, and versatile surface modification. We systematically investigate the effect of fabrication parameters, such as laser beam power and scanning velocity, on the quality, thickness, and topography of the resulting microelements. To highlight the versatility of DLW, we present examples of 2D and 3D mussel-inspired material patterns in terms of fabrication resolutions and potential applications. We achieve the spatial resolutions of 250 ± 20 nm for MI-dPG and 2.1 ± 0.1 µm for PDA and demonstrate for the first time the fabrication of 3D MIM microstructures that easily exceed 20 µm in height.

The post-functionalization capabilities of MIM microarchitectures are demonstrated by metallization of the microstructures and an extended study on immobilization of poly-adenine and poly-thymine single-stranded DNA. First, we tested the direct attachment and affinity of a Cy5 labeled single-stranded DNA (ssDNA-Cy5) probe under diverse conditions. Subsequently, a facile DNA detection method of poly-thymine oligonucleotide is developed based on selective hybridization with complementary poly-adenine immobilized on the MI-dPG micropattern surface. To demonstrate the potential for miniaturization, we demonstrate DNA sensing using the DLW fabricated MIM nanoarray. MI-dPG can be also easily functionalized with silver particles by the reduction of Ag^+ from solution by catechol groups. The DLW micropatterning of MIM materials presented in this work empowers further development of bio-microarrays. Moreover, the mussel-inspired microstructured materials that can be realized based on our work provide a versatile platform for high-precision selective surface functionalization, which could find applications in miniaturized systems.

2. Results and Discussion

Mussels can strongly adhere to almost any surface due to the underlying biochemistry of byssus plague. The mussel foot proteins (MPFs) present in the plague have a high amount of amine and catechol groups, which play the key role in the binding mechanism. Inspired by the chemistry of MPF, materials such as dopamine, synthesis-designed mussel-inspired linear polyglycerol, and dendritic polyglycerol (**Figure 1a**) were subjected to micropatterning with Direct Laser Writing. DLW is based on focusing the NIR fs laser beam at the interface between the glass substrate and the MIM solution (Figure 1b). The micropatterning was performed in the presence of 2,5-bis[4-[N, N-bis-[2-(acetyloxy)ethyl]phenyl]-methylene]-(2E,5E) cyclopentanone (BAE) photoinitiator in the pH range of 7.0–8.5 using different buffers depending on the MIM material formulation. After adjusting the fabrication conditions, the produced micropatterns were tested for their ability to be post-functionalized with single-stranded DNA and silver ions, as shown schematically in Figure 1c.

2.1. Formation of MIMs Micropattern

To evaluate the DLW fabrication window, the micropatterning of PDA, MI-lPG, and MI-dPG was carried out at different laser powers and scanning velocities in the range of 5–30 mW and 50–250 µm s^{-1}, respectively, resulting in an array of simple cubic structures as shown in **Figure 2a,1**.

PDA fabrication was tested in the presence of different buffers such as 0.1 M tris(hydroxymethyl)aminomethane (Tris) buffer at pH 7.0 and pH 8.5, and 0.1 M phosphate buffer at pH 8.5. 0.1 M (3-(N-morpholino) propanesulfonic acid (MOPS) buffer at pH 8.5 was used for the micropatterning of MI polyglycerols. As a result, PDA patterns can be fabricated from all three solutions mentioned above (Figures S1–S3, Supporting Information). It appears that the PDA patterns have a grain-like morphology with the different packing densities, which can be tuned by adjusting the beam scanning velocity and laser exposure power. In general, we obtained denser structures at higher powers and slower laser scanning velocities. On the other hand, the pattern density decreases rapidly with increasing laser velocity and soon leads to no visible PDA formation. This can be explained by the nature of PDA build-up, which is based on both covalent oxidative polymerization and non-covalent self-assembly.[21,24] These processes are relatively slow when compared to radical and cationic polymerization, which can typically be achieved with scanning velocities in the order of thousands of microns per second. Comparing different fabrication conditions and buffer media

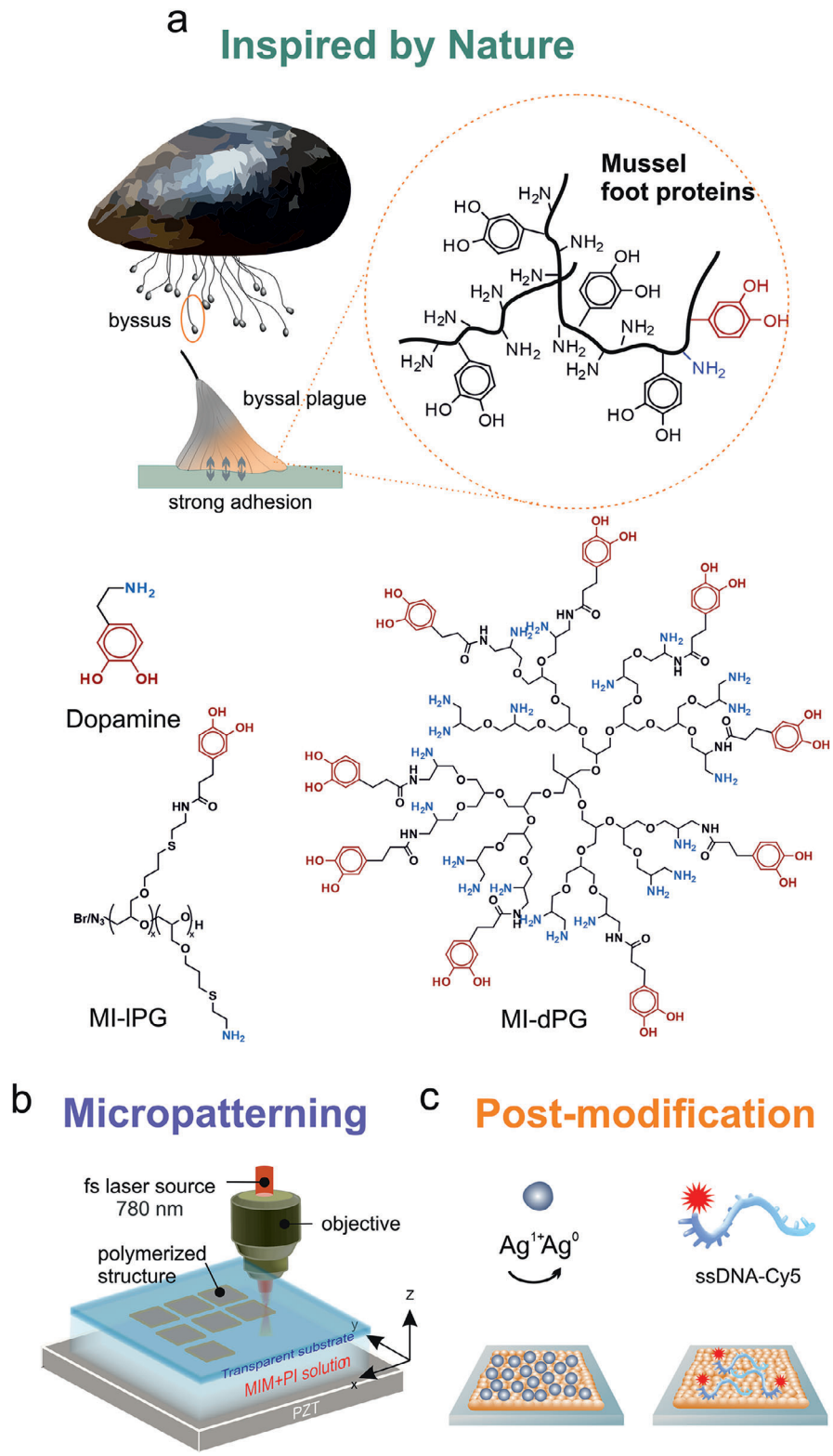

Figure 1. Micropatterned nature-inspired functional surfaces. a) Inspired by Nature. Top: Mussel adhesion concept based on the chemical structure of mussel foot proteins present in a byssus plague. Simplified MPF structure with amine and catechol groups highlighted, which play a key role in binding the mussel to the surface. Bottom: the chemical mimicry of dopamine, synthesis-designed mussel-inspired linear , and dendritic polyglycerols . b) Micropatterning, Schematic concept of micropatterning of mussel-inspired materials by multiphoton Direct Laser Writing from solutions of mussel-inspired materials (MIMs) and photoinitiator (PI). Movement of the focal spot in the material solution results in the formation of 2D MIM microstructures. c) Post-modification Post-functionalization of MIM micropatterns for (left) immobilization of silver nanoparticles and (right) DNA sensing by attachment of cyanine-5 labeled single-stranded DNA. For details see the text.

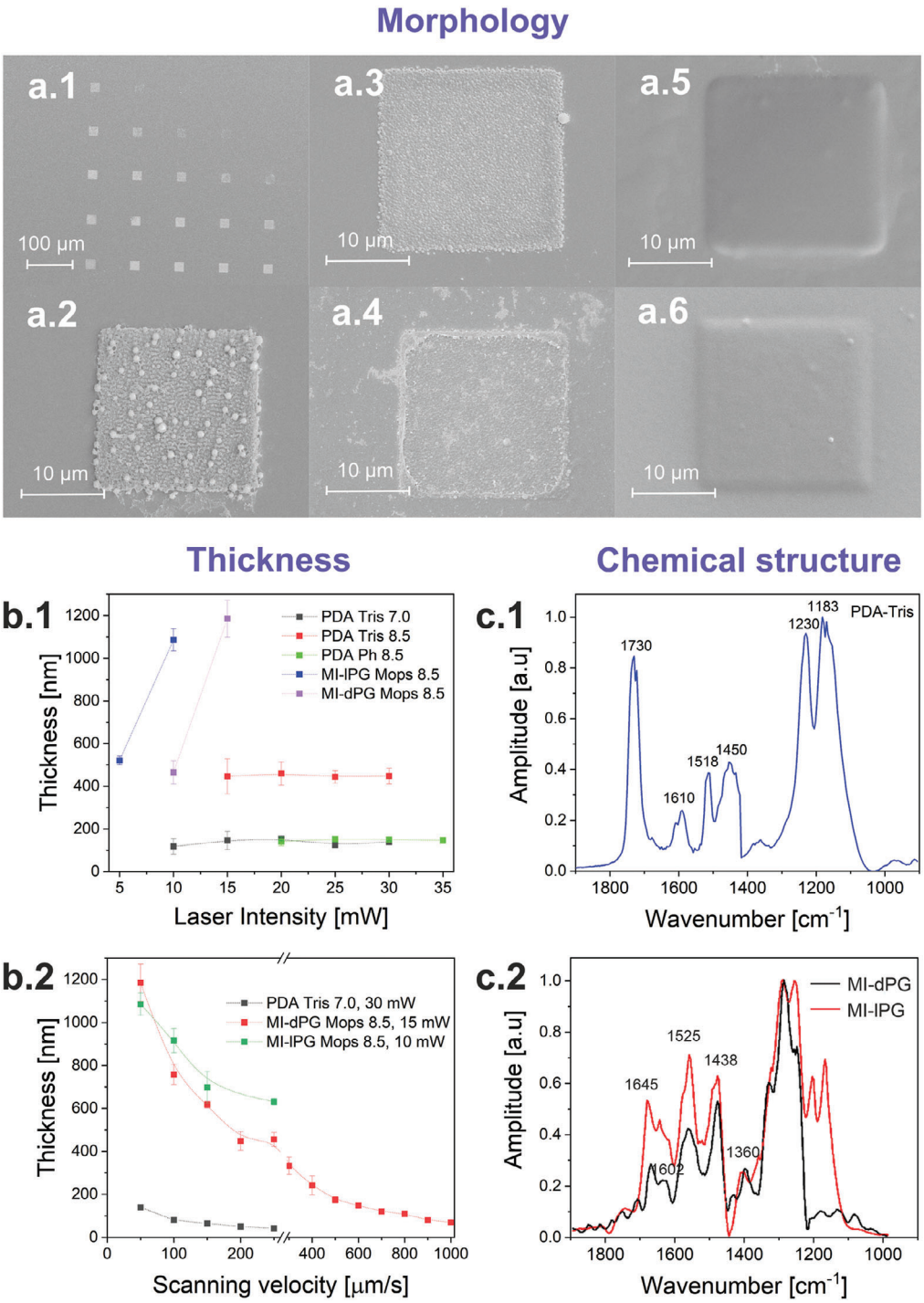

Figure 2. Morphology, thickness, and chemical composition of MIM microstructures. a) Scanning electron microscope micrographs of an exemplary MIM micropatterns: a.1, overall view of calibration array with alternating laser power (top-down) and velocity (left-right); a.2, DLW pattern of PDA Tris buffer, pH 8.5 (30 mW, 50 µm s^{-1}); a.3, PDA Tris buffer, pH 7.0 (30 mW, 50 µm s^{-1}); a.4, PDA phosphate buffer, pH 8.5 (30 mW, 50 µm s^{-1}); a.5, MI-IPG MOPS buffer, pH 8.5; a.6, MI-dPG MOPS buffer, pH 8.5. b) Thickness of the MIM patterns produced at: b.1, fabrication speed of 50 µm s^{-1} and different laser intensities; b.2, different scanning velocities. Laser powers are mentioned in the capture for each MIM solution. Dashed lines are a guide for the eye. c) Chemical structure: c.1, AFM-based infrared spectra of PDA patterns produced from 0.1 M Tris buffer, pH 8.5; c.2, MI-dPG (black) and MI-IPG (red) from 0.1 M MOPS buffer, pH 8.5.

used (Figure 2a,2–4), we selected 0.1 M Tris pH 7.0, for further material investigation based on the quality of the patterns obtained.

Furthermore, the DLW of MI polyglycerols showed a narrow fabrication power window of 10 to 15 mW, although a wider range of scanning velocities resulted in micropattern formation (Figures S4–S5, Supporting Information). MI-dPG patterns can be fabricated at velocities up to 1000 μm s^{-1}, whereas high-density PDA patterns can only be fabricated with 150 μm s^{-1}. This is a major advantage of MI-dPG over PDA, as the micropatterning throughput of this material is at least four times higher. This is due to the much higher molecular weight of the MI-dPG compared to the small PDA molecule (Figure 1a). In contrast to PDA, both linear and dendritic structures exhibit a continuous, smooth surface morphology for all patterns despite varying fabrication parameters.

During PDA microstructuring we obtained patterns up to 440 nm in thickness, as seen for alkaline Tris buffer solutions (Figure 2b), while only 120 to 150 nm could be reached from other solutions. On the other hand, the micropatterns of MI polyglycerols exhibit much higher thicknesses than those of PDA, reaching 1.1 and 1.2 μm for MI-lPG and MI-dPG, respectively. In general, a decrease in the thickness with increasing scanning velocity is observed for all materials studied (Figure 2b,2). In conclusion, the thickness of the MIM micropatterns can be tailored by varying the laser scanning velocity and, in the case of PDA, by the pH of the solution.

Next, we investigated the chemical composition of micropatterns using of AFM-based infrared spectroscopy (AFM-IR). This technique was chosen because it overcomes the spatial limitations of conventional IR microscopy by providing information from surfaces as small as 30 nm^2, making it a perfect tool for studying micro-sized objects.[25] The spectra recorded at the micropatterned area reveal the characteristic peaks of the corresponding MIM materials (Figure 2c). The spectrum of DLW micropatterned PDA can be compared with those from previous studies on conventionally obtained PDA[26,27] as well as to DLW structure.[23] The peaks at 1610 and 1518 cm^{-1} indicate the ring structure of the benzene and nitrogen heterocycle of PDA. Absorption in 1453–1426 cm^{-1} range corresponds to C—H stretching and 1730–1722 cm^{-1} to the C═O vibration in quinone structures of PDA. Another origin of the 1730 peak can be assigned to the BAE photoinitiator added to the solution to enable the sensitivity to the NIR laser.

The chemical composition of MI-PG micropatterns is in the good agreement with the conventionally polymerized material[14] (Figure 2c,2). The peaks at 1100–1200 cm^{-1} are ascribed to C—O while the O—H bonds present in the catechol groups of MI-PG can be detected in the region of 1360 cm^{-1}. The peak within the range of 1370–1400 cm^{-1} belongs to C—H vibrations of the backbone. The C—H bonds of quinones in covalently crosslinked MI-PG give a peak at 1438 cm^{-1}. The strong signal at 1525 cm^{-1} is the vibrational band of amide II present in the MI-PG microstructure. The weaker signal at 1602 cm^{-1} is assigned to the C═C vibrations of the phenyl in the catechol groups, indicating partial oxidation of the catechol groups to quinone. The observed peak at 1645 cm^{-1} is a characteristic signal for quinines, C═C and C═O of the quinone, and amide I. The presence of amide I and II reveals the Michael addition and Schiff base reactions during crosslinking as mentioned above.[28] The presented AFM-IR spectra show similarities with the reported IR characterization of conventionally polymerized MI-dPG.[14]

2.2. High Precision Microstructuring

2.2.1. 2D Fabrication

To demonstrate the resolution of DLW patterning and the versatility of 2D design provided by DLW, we fabricated arrays of single lines from MIMs and the exemplary intricated 2D patterns (**Figure 3**). The series of experiments on single-line arrays revealed that increasing the laser power or decreasing the scanning velocity results in the wider patterns (Figure 3a, Figure S6, Supporting Information). This is a common observation in DLW, which is caused by the increase in voxel volume and material exposure dose. While line widths up to a few micrometeres can be achieved at slower laser velocities (e.g., Figure 3a,2), the thinnest single MI-dPG line of 250 ± 20 nm is obtained after speeding up the fabrication to 250 μm s^{-1}. In the case of PDA micropatterns, we achieved the line width of 2.1 ± 0.1 μm, which can be then increased by decreasing the laser velocity (Figure S6, Supporting Information). The presented DLW resolution of MIM micropatterning allows us to achieve high-precision surface modification in miniaturized systems and microdevices. Furthermore, we can see that by tuning the DLW fabrication parameters, the throughput and precision of the micropatterning can be adjusted according to the task at hand.

Figure 3b–d demonstrates the versatility of DLW 2D patterning. The good structure quality can be observed for all three MIM microstructures when compared to the STL files used. For example, the MI-lPG pattern with details in the range of 5 μm and for PDA ≈ 4.2 μm are in a good agreement with the structural properties as defined during the design process.

2.2.2. 3D Fabrication

Next, we attended the fabrication of 3D microstructures of MIMs. Unfortunately, it was not possible to obtain 3D features using PDA. This was mainly attributed to the low structural stiffness resulting from the nature of interactions in PDA materials[29] and the insufficient occurrence of polymerization events to establish a resilient 3D material network. In contrast, 3D microstructuring is possible with much larger molecules such as MI-dPG. First, we evaluated the range of laser powers and velocities to achieve optimal fabrication conditions for MI-dPG (Figure S7, Supporting Information). Too little exposure leads to insufficient build-up of the matter, while too much exposure produces oversized structures with distorted shapes. Examples of 3D microstructures fabricated with optimized fabrication patterns show good structural quality (**Figure 4**): a pyramid array with an approximate height of 20 μm can be used to create a lotus-like surface (Figure 4a, Video S1, Supporting Information); basket-like honeycomb structures that provide a confined volume that can be used for detection, for example, by efficiently isolating and trapping a single cell in each honeycomb hole (Figure 4b,

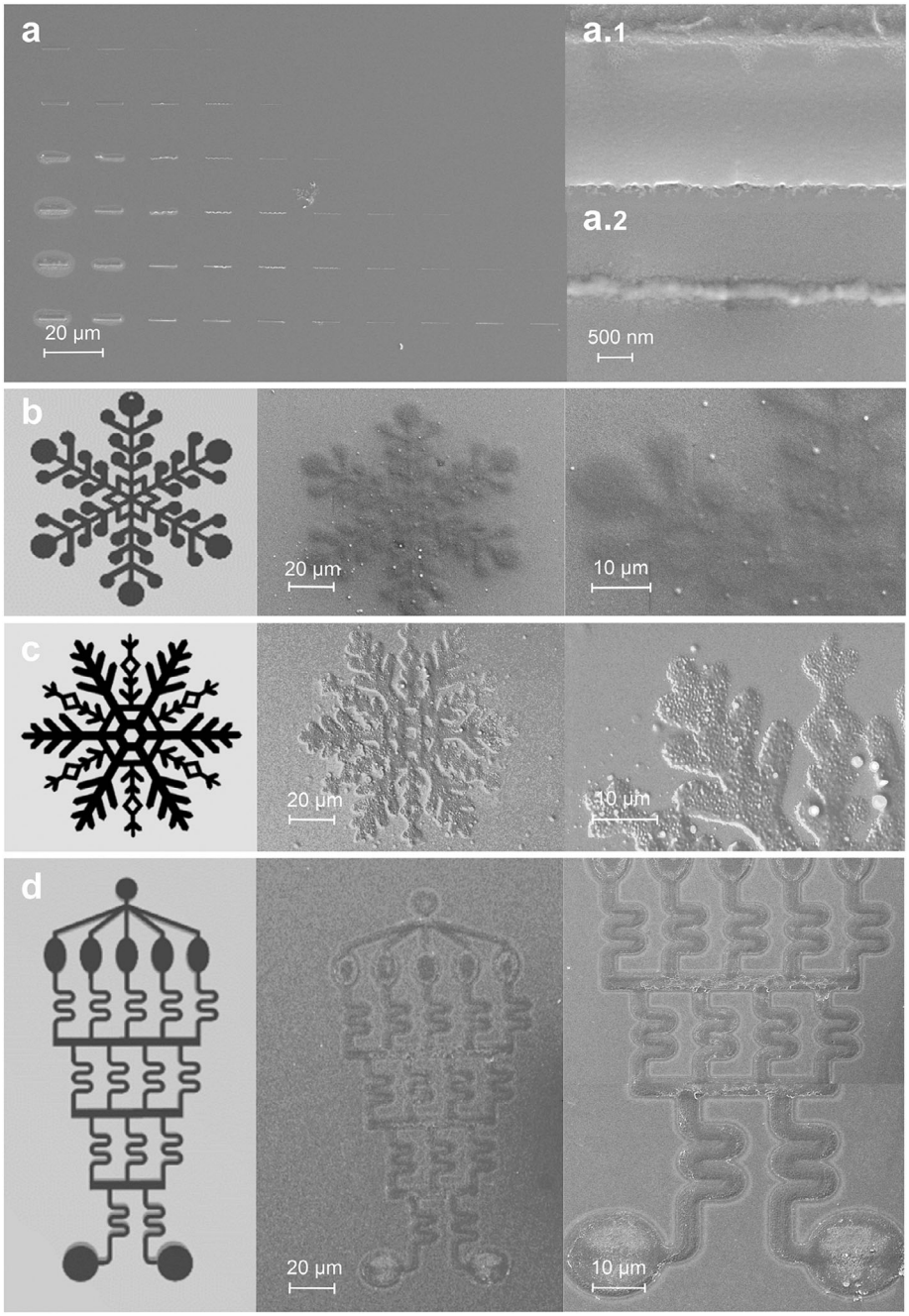

Figure 3. DLW resolution and versatility of 2D micropatterning. Scanning electronic microscope micrographs of (a), array of single lines of MI-dPG, MOPS pH 8.5 for 5–30 mW (increases from top to down) and 25–250 µm s^{-1} (increases from left to right): a.1, 10 mW, 25 µm s^{-1}; a.2, 25 mW, 250 µm s^{-1}. 2D micropatterns of (b), MI-dPG, MOPS pH 8.5, 12 mW, 100 µm s^{-1}; c) MI-lPG, MOPS pH 8.5, 12 mW, 70 µm s^{-1}; d) PDA, Tris buffer pH 7.0, 30 mW, 100 µm s^{-1}.

Video S2, Supporting Information);[30] a pillar microarray, a design we further applied for DNA detection (Figure 4c, Video S3, Supporting Information). For applications in sensing, such MI-dPG 3D structures can be directly DLW deposited onto superhydrophobic substrates specifically developed for the fabrication of DNA microarrays, to avoid unspecific attachment of the analyte molecule to the substrate (Figure S8, Supporting Information).

2.3. Immobilization and Detection of DNA

DNA detection is of paramount importance in various fields including molecular biology, medicine, genetics, forensics, biotechnology, and environmental monitoring. Much attention has been given to the fabrication of biological microarrays, as miniaturized devices capable of efficiently characterizing biological samples including proteins, RNA, and DNA sequences. This technology

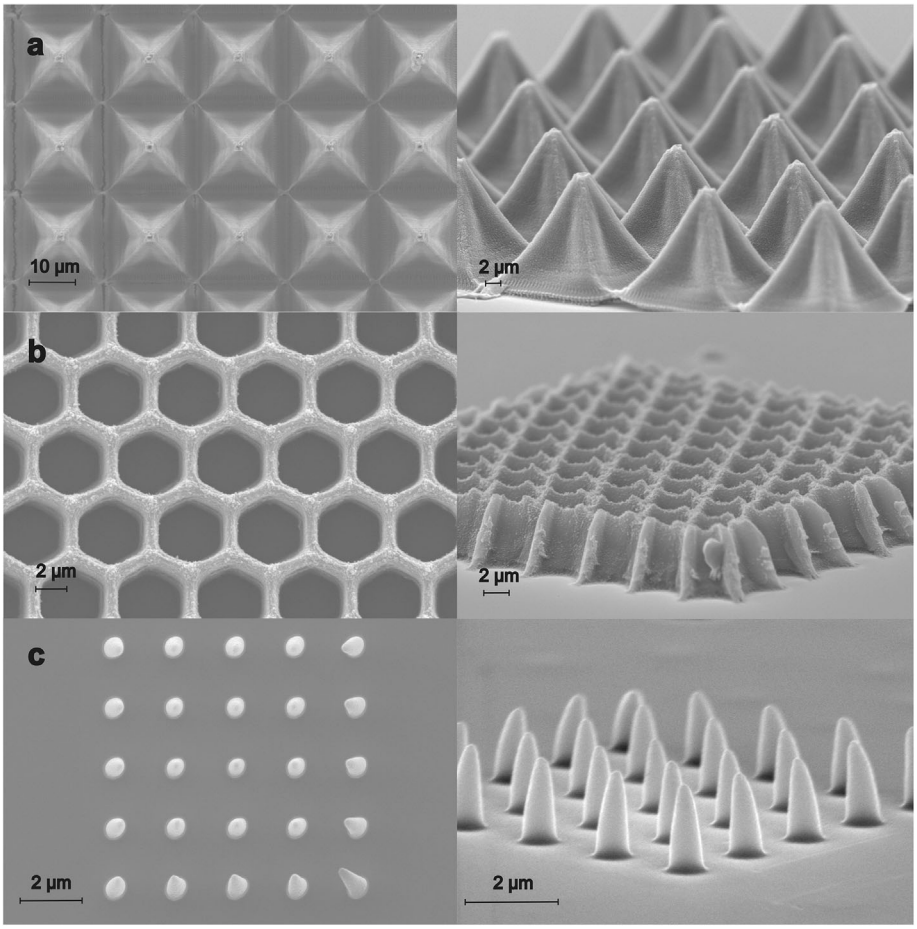

Figure 4. 3D microstructuring. a) Pyramid array mimicking lotus surface. b) Honeycomb. c) Microarray. MI-dPG, 0.1 M MOPS buffer at pH 8.5. 20 mW, 300 µm s^{-1}.

exhibits high throughput, sensitivity, and specificity provided by the array design of numerous micro- or nano-sized features consisting of biological components (e.g., protein or DNA). Some of the key aspects in the biosensor development are high reproducibility and the ability to generate micro- to nanostructures.[31] To date, the major fabrication challenges are attributed to the creation of biochemical patterns/structures at the desired location with precise design architectures (i.e., size, shape) and the retention of their bioactivity. Furthermore, the demand for high-sensitivity multicomponent analysis with the limited amount of the sample has driven the further development of micro/nanofabrication protocols,[31–33] high-density array designs,[34] and single-cell sequencing.[35]

The DLW capabilities of MIM microstructuring, as demonstrated in the previous chapter provide a solid platform for the production of micro- and nano-arrays. In addition, MIM are perfect candidates for a versatile choice of hybridization agents to tailor for selective detection of target DNA.

Double-stranded and single-stranded DNA (ssDNA) of various lengths have been applied in DNA-based bio-dosimetry, data storage, biotechnology, pharmaceuticals, and DNA-based functional nanomaterials.[36] For example, surface-deposited DNA has been used to investigate the radiation response of biomolecules in cancer research.[37,38] To demonstrate the capability of DLW fabricated MIM microstructures for selective post-functionalization and DNA sensing, we immobilized fluorescence-labeled poly-adenine and poly-thymine ssDNA probes on our fabricated micro- and nanostructures.

First, we investigated the binding affinity of ssDNA consisting of poly-adenine labeled with a Cy5 fluorescent dye (*poly*-A-Cy5) on MIM micropattern surfaces testing both polydopamine and MI-dPG, various substrate modifications, detection conditions, and post-immobilization treatment of the pattern surface (**Figure 5**). The presence of the labeled nucleotide was detected using a fluorescence array scanner.

To analyze polydopamine, we chose 635 nm as the excitation wavelength since it corresponds to the maximum of Cy5 absorption and, importantly, the PDA micropatterns do not show any autofluorescence emission signal (Figure S9, Supporting Information). After the immobilization step, *poly*-A-Cy5 can be observed on both, the PDA microstructures and the glass substrate (Figure 5b left); therefore, an additional sonication of the substrate in phosphate buffered saline (PBS) was performed to remove the non-specifically bound oligonucleotides from the glass substrate itself. This step removed most of the *poly*-A-Cy5 around the PDA patterns, but also resulted in a noticeable decrease in

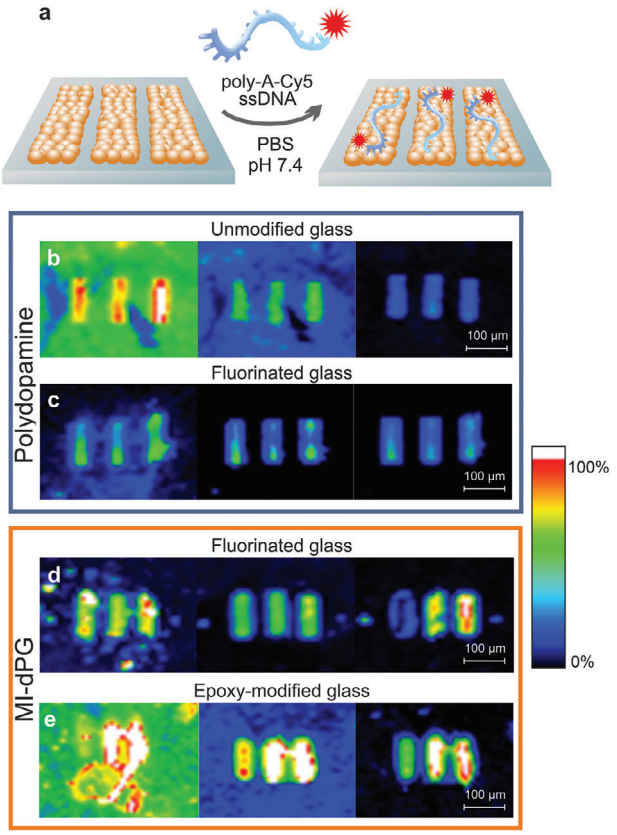

Figure 5. DNA sensing. a) Schematic of the cyanine-5 labeled poly-adenine immobilization on the surface of mussel-inspired micropatterns. b–e) Fluorescence images of MIM microstructures at 635 nm (left) after poly-A-Cy5 ssDNA incubation and rinsing with PBS buffer, (middle) after additional 15 min of sonication in PBS buffer, (right) and additional 15 min sonication in PBS buffer and 5 min in acetone. b) PDA on unmodified glass, incubation time 15 min. c) PDA on fluorinated glass, incubation time 60 min. d) MI-dPG on fluorinated glass, incubation time 15 min. e, MI-dPG on epoxide-functionalized glass, incubation time 15 min. The color scale bar represents the percentage of fluorescence intensity. Detector signal gains are 50 for PDA and 20 for MI-dPG. Used poly-A-Cy5 concentrations: 60 mM for PDA and 20 mM for MI-dPG.

fluorescence intensity on the PDA micropatterns themselves, indicating partial detachment of the *poly*-A-Cy5 strands (Figure 5b middle, right). To improve the attachment, we attempted to improve immobilization through the addition of divalent cations, however, it led to a loss of specificity between the glass substrate and PDA patterns (Figure S10, Supporting Information). We were able to achieve a significant reduction of the attachment of DNA to the glass substrate by fabricating PDA micropatterns on hydrophobic fluorinated glass (Figure 5c). Extended sonication leads to improved signal-to-noise ratio that improves the sensitivity of the DNA detection.

Similar to PDA, MI-dPG structures were excited at 635 nm for DNA detection due to little to no autofluorescence (Figure S11, Supporting Information). We tested epoxide- and fluoride-modified glass substrates for immobilization of *poly*-A-Cy5, as the use of unmodified glass results in significant saturation of the substrate despite extensive cleaning (Figure S12, Supporting Information). ssDNA-modified MI-dPG shows a strong fluorescence signal even at *poly*-A-Cy5 concentration three times lower than that used for immobilization on PDA. This indicates a better affinity of DNA with MI-dPG (Figure 5d,e). Furthermore, no obvious decrease in fluorescent intensity of the micropatterns is observed during extensive washing, indicating a strong interaction between ssDNA and MI-dPG.

In summary, although PDA can be used for DNA attachment, MI-dPG based microstructures show more potential for the development of DNA sensing methods. Considering also the better fabrication throughput of MI-dPG, we selected this material to investigate, first, whether it can be used for specific DNA hybridization and, second, to evaluate whether it can be used for quantitative DNA detection. To this end, we first modified the MI-dPG micropattern surface with an adenine-based nucleotide (*poly*-A) that is complementary to and specifically binds to the cyanine-5 labeled poly-thymine (*poly*-T-Cy5) DNA target (**Figure 6a**). Representative images of MI-dPG-poly-A before and after hybridization with *poly*-T-Cy5 show an increase in fluorescence with increasing concentration of target DNA (Figure 6b,c).

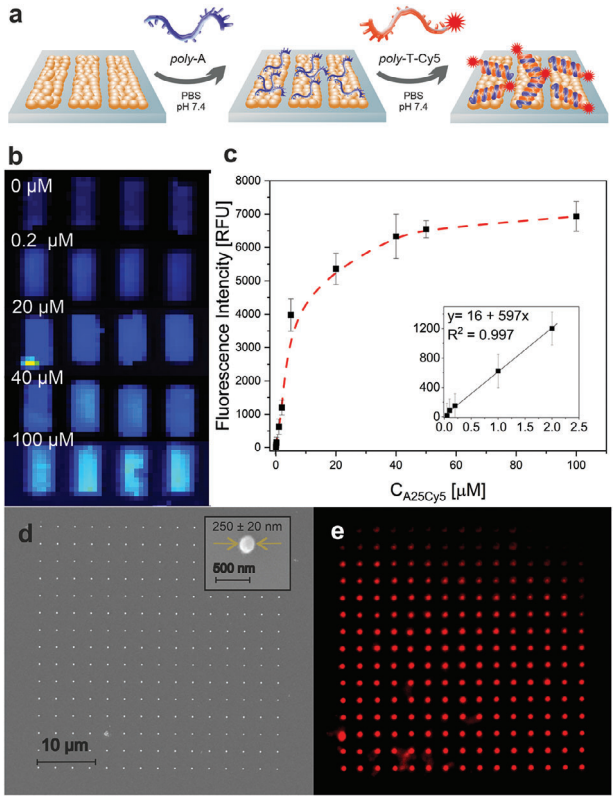

Figure 6. DNA detection. a) Schematic of the cyanine-5 labeled T25mer poly-thymine immobilization on the surface of mussel-inspired micropatterns hybridized with 50 µM A25 oligonucleotide (MI-dPG-poly-A). b) Fluorescence images of MI-dPG-poly-A capture micropattern before and after poly-T-Cy5 immobilization. Detection signal gain is 5. Image intensity threshold for all images is 0–150 for better visual comparison. c) Concentration-dependent fluorescence intensity signal of poly-T-Cy5 (50–100 µM) immobilized on MI-dPG-poly-A. RFU stands for relative fluorescence units. d) Scanning electron micrograph of MI-dPG nanoarray. e) Fluorescence signal of the same nanoarray after immobilization of poly-T-Cy5 (10 µM, 30 min). The image shown in the red channel with an intensity threshold set at 25–70 RFU for better contrast with the eye.

We confirmed the specific binding of *poly*-T-Cy5 to the immobilized *poly*-A by showing that *poly*-A-Cy5 shows no significant evidence of binding (Figure S13, Supporting Information). To check the melting behavior of poly-A and poly-T, we boiled the samples with immobilized DNA in PBS. This resulted in partial melting of the DNA (Figure S14, Supporting Information). A quantitative analysis of the hybridization efficiency at different *poly*-T-Cy5 target probes shows a linear dependence in the concentration range of 0.05–5.0 μM (Figure 6c insert). This means that the MI-dPG microarray can be successfully used for the quantitative and sequence-specific detection of DNA. However, further increase of the target concentration leads to the saturation effect. The current LOD is limited by the accuracy of our instrument, and we believe that further adjustment of the detection protocol, such as capture oligonucleotide concentration, hybridization temperature, and post-hybridization treatment of the microarray, could significantly improve the range of detected concentrations.

Scaling down in the size of array sports is desired to improve assay signal and rapidity,[39] reduce probe volume, and to allow for a higher density of specific probes and thus a wider range of targets that can be detected per microchip device. As a proof-of-concept for the potential miniaturization and applications of DLW-fabricated MIM, we fabricated a MI-dPG nanoarray of 15 × 15 pillars with a diameter of 250 ± 20 nm and performed oligonucleotide immobilization using the same protocol as in the case of micropatterns (Figure 6d,e). The fluorescence intensity of MI-dPG-*poly*-A increased from 7.0 ± 0.5 to 65 ± 5 RFU after hybridization with 10 μM *poly*-T-Cy5, demonstrating the potential for further development of MIM-based nanoarrays for DNA detection.

2.4. Silver Immobilization

The high reduction potential of quinone groups and the metal binding ability of mussel-inspired polymers can be utilized for direct synthesis and subsequent electroless deposition of metal nanoparticles without further reducing agents or metal seed particles.[21,18] We tested the ability of DLW-fabricated PDA and MI-dPG micropatterns to serve as a suitable silver immobilization agent. Energy dispersive X-ray spectroscopy (EDX) spot measurement and cross-sectional scanning revealed no noticeable presence of silver on the PDA pattern surface. Moreover, only 0.11% of Ag is detected on the autooxidized PDA coating (**Figure 7a,b**; Figure S15, Supporting Information). In contrast, an Ag peak is clearly observed for MI-dPG at 2.984 keV with nanoparticles detected on the pattern surface (Figure S16, Supporting Information). Remarkably, MI-dPG micropatterns show an Ag content of 15.8%, which is a significant increase compared to autooxidized PDA (Figure 7b; Figure S15, Supporting Information). In addition, the cross-sectional EDX study of MI-dPG revealed the presence of silver on the entire profile of the microstructure (Figure 7c,d), while none was found on the substrate surface. It can be seen that the decrease in the elemental contents representing the borosilicate glass substrate, such as Si, O, and Na, is followed by an increase in the carbon content, indicating the organic nature of MI-dPG on the glass, and an increase in a signal from deposited silver.

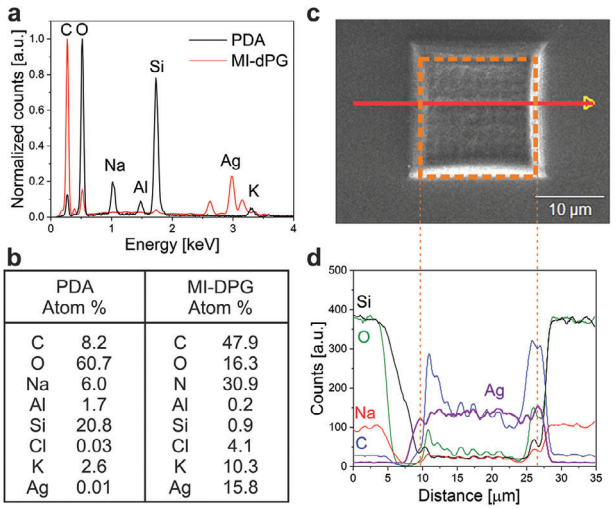

PDA Atom %		MI-DPG Atom %	
C	8.2	C	47.9
O	60.7	O	16.3
Na	6.0	N	30.9
Al	1.7	Al	0.2
Si	20.8	Si	0.9
Cl	0.03	Cl	4.1
K	2.6	K	10.3
Ag	0.01	Ag	15.8

Figure 7. Silver immobilization. a) EDX spectra of PDA and MI-dPG pattern surfaces after Ag immobilization. b) Elemental quantitative data representative. c) SEM micrograph of MI-dPG pattern and the representation of cross-sectional EDX analysis. d) Space-resolved elemental information from the cross-sectional EDX scan. Dashed lines between c and d figures are a guide for the eye between the edges of MI-dPG structure and EDX signal profile. Borosilicate glass was used as the substrate.

We cannot exclude the presence of silver on the PDA micropatterns based on the EDX results alone. However, under the given experimental conditions, the MI-dPG surface possesses a much higher reduction potential than the PDA micropatterns and autooxidized coatings. As a result, MI-dPG can be used for a one-step facile and precise Ag electroless metallization. This can be used in the microfabrication of circuits and other conductive micro-elements, or in the creation of high surface area antimicrobial surfaces.

3. Conclusion

In this work, we demonstrate the micropatterning approach of mussel-inspired materials that overcome the limitations of existing deposition techniques. We can readily achieve MIMs microstructures with 2D and 3D intricate designs and reach the resolution of 250 ± 20 nm and 2.1 ± 0.1 μm for MI-dPG and PDA for DLW micropatterning. While the chemical composition of all DLW micro-patterns was confirmed by AFM-IR, we demonstrated that the pattern topography, resolution, and throughput of MIM DLW micropatterning can be easily tuned by varying the laser power, scanning speed, and solution formulation. For MIM patterning, a range of morphologies has been demonstrated, from the grain-like morphology inherent to PDA to the continuous smooth morphology of MI-PG. However, up to now, the DLW of PDA is limited to 2D deposition in the range of up to 450 nm thick patterns and a fabrication throughput of up to 250 μm s^{-1}. Unlike PDA, MI-dPG can be patterned in 2D and 3D at higher laser scan speeds without sacrificing surface quality.

The potential for DNA sensing of the MIM micropatterns was confirmed by the successful immobilization of poly-adenine and poly-thymine ssDNA as detected by fluorescence scanning

spectroscopy. Both, PDA and MI-dPG show successful attachment of ssDNA, but the later shows higher oligonucleotide attachment efficiency, which is stable during further sample processing steps. Subsequently, we demonstrate that MI-dPG micropatterns functionalized with ssDNA probes can be used to detect DNA with high specificity and sensitivity. The presence of ssDNA was detected at concentrations as low as 50 nM. As an example of further miniaturization, we demonstrate a DLW fabricated MI-dPG nanoarray with a single spot size of 250 nm for successful DNA detection. The MIM fabrication platform realized in this work can greatly contribute to the development of bio-nanoarrays. The one-step facile Ag immobilization results in high metal particle coverage and can be applied for electroless metallization in complex microdevices. Considering the pattern quality, fabrication throughput, and post-immobilization capability, the dendritic polyglycerol derivative is the best candidate for 2D and 3D high-precision DLW fabrication and further functionalization. In conclusion, the presented microfabrication approach of multifunctional MIM materials provides us with an excellent concept for the precise, highly controlled functionalization of various substrates and miniaturized devices (e.g., microfluidics, lab-on-chip, and other MEMS).

4. Experimental Section

Solution Preparation: Dopamine hydrochloride (Sigma-Aldrich) 7.15 mM solutions were prepared in 0.1 M solution of tris(hydroxymethyl)aminomethane buffer (pH 7.0 and 8.5, Alpha Aesar) and 0.1 M phosphate buffer (pH 8.5, Alpha Aesar). Mussel-inspired linear polyglycerol with 80% catechol and 20% amine functional groups and dendritic polyglycerol (Mn = 5000 g mol^{-1}, Mw = 7500 g mol^{-1}) with 40% catechol and 60% amine functional groups were synthesized as described elsewhere.[14,40] 3.7 M and 4 M solutions of MI-lPG and MI-dPG, respectively, were prepared in mixture of 0.1 M solution of 3-(N-morpholino) propane sulfonic acid (pH 8.5, Alpha Aesar) and methanol in a volume ratio of 1:4. All the resulting solutions were stirred for 15 min and then an aliquot of 2,5-bis [4-[N, N-bis-[2-(acetyloxy)ethyl]phenyl]-methylene]-(2E,5E)-cyclopentanone (GenoSynth GmbH, Berlin, Germany) photoinitiator solution in acetone was added, resulting in a final photoinitiator concentration of 2 wt.%. The obtained mixtures were stirred for 2 h and further subjected to the DLW microfabrication step.

Conventional coating of PDA was prepared by dissolving dopamine hydrochloride in a 0.1 mol L^{-1} Tris buffer at a concentration of 1 mg mL^{-1}. Glass coverslips were immediately immersed in the solution for 15 h at room temperature. The samples were then withdrawn, rinsed thoroughly with water, and dried with nitrogen.

Silanization Procedure: High-precision coverslips with the thickness of 0.170 ± 0.005 mm (Paul Marienfeld GmbH) were washed by ultrasonication in dimethyl sulfoxide (Chemsolute) for 15 min and rinsed with MiliQ water. Next, they were sonicated in acetone for 15 min, rinsed, and dried under pressurized nitrogen. For MI-dPG micropatterning, the cleaned glass slides were immersed in a solution of trimethoxy [2-(3,4-Epoxycyclohexyl)ethyl] trimethoxysilane (Sigma–Aldrich) in dichloromethane (Sigma–Aldrich) at volume ratio of 1:100 for 24 h. The glass slides were then rinsed with dichloromethane and dried under a nitrogen stream.

For fluorinated surfaces, the cleaned glass slides were exposed to oxygen plasma for 10 min at 60 W and then immediately placed in a Petry dish containing 50 µl of perfluorooctyl-trichlorosilane (Sigma–Aldrich) for 2 h. Subsequently, the glass slides were washed by sonication in acetone for 15 min and dried under a nitrogen stream.

Direct Laser Writing: Laser nanofactory machine from Femtika Ltd. (Vilnius, Lithuania) was used for multiphoton DLW for PDA and MI-dPG micropatterning. The machine is equipped with an Erbium-doped fiber laser (Menlo, Germany) emitting at 780 ± 10 nm and with a pulse duration of <100 fs and a repetition rate of 100 ± 1 MHz. The XYZ linear stages are synchronized with the galvano scanners responsible for the movement of the laser beam. An extra-long distance air objective (20 ×, 0.45 numerical aperture, Plan Fluor, Nikon, Tokyo, and Japan) was used. The effect of laser power and velocity on micropatterning was studied in the range of 5–30 mW and 50–1000 µm s^{-1}, respectively. To ensure homogeneous overlap, the hatching and slicing steps were set to 0.2 and 0.5 µm, respectively. All structures were fabricated with the first layer in contact with the substrate and further slicing layers were produced in the direction into the MIM solution. The writing process was controlled by the *3DPoli* software, which had the ability to import an STL file using the internal programming language that allowed the structure to be designed by code and variables. The STL files used were taken from the open sources www.thingiverse.com and www.grabcad.com.

To proceed with polymerization, the resulting solution was placed between two glass slides using a silicon spacer. After DLW fabrication, the samples were developed in methanol for 2 h and then sonicated in acetone for 10 min and dried under N_2 flow.

DNA Immobilization: For this experiment, MIMs micropatterns with a size of 100 × 30 µm and a distance of 50 µm from each other were fabricated by DLW on the glass substrate. PDA and MI-dPG micropatterns were produced at 30 mW, 100 µm s^{-1} and 20 mW, 300 µm s^{-1}, respectively.

To investigate the affinity of DNA to patterns, PDA and MI-dPG micropatterns were incubated in 60 and 20 µM of cyanine-5 labeled polyadenine 36mer (*poly*-A-Cy5) (Thermo Fisher Scientific GmbH, Germany) in PBS solution at pH 7.4 (Alpha Aesar), respectively. After 15 min of incubation, the PDA micropatterns were washed with PBS buffer, followed by 15 min of sonication in PBS, and finally 5 min of sonication in acetone.

For quantitative detection of the cyanine-5 labeled T25mer poly-thymine (*poly*-T-Cy5), we prepared solutions at different concentrations from 0.05 to 100 µM of *poly*-T-Cy5 (Thermo Fisher Scientific GmbH, Germany) and 10, 50, 100 µM of complementary oligonucleotides A25 (*poly*-A) and A25-Cy5 (*poly*-A-Cy5) in 0.1 M PBS at pH 7.4 (Sigma Aldrich). Each incubation step was performed for 30 min at 23.5 °C and 35% RH. Incubation was followed by washing in the flow of PBS for 2 min and in the flow of MiliQ water for 5 min. To test the hybridization of (*poly*-T-Cy5) target DNA we first immobilized the surface of MI-dPG micropatterns and nanoarrays with sequence matched 50 µM *poly*-A capture DNA.

Silver Immobilization: 50 mM silver nitrate solution (Chemsolute, Germany) was prepared in MiliQ water. After the DLW step, the glass slides with freshly fabricated MIM micropatterns were immersed in in 50 mM aqueous solution of $AgNO_3$ for 18 h, then rinsed with MiliQ water and dried at room temperature with nitrogen flow.

Characterization Methods: Scanning Electron Microscopy was used to investigate the morphology and overall quality of the micropatterns. The samples were sputtered with a 15 nm thick gold layer and the micrographs were obtained using an EVO MA 10 SEM unit (Carl Zeiss Microscopy GmbH, Germany) with a secondary electron detector. An accelerating voltage of 10 kV was used.

Energy-dispersive X-ray Spectroscopy was applied to analyze the chemical composition of the micropatterns after silver immobilization. The samples were coated with a 15 nm thick carbon layer and analyzed with a Pathfinder Basecamp EDX system equipped with a silicon-drift detector (Pathfinder System, Thermo Scientific) coupled with the EVO MA 10 SEM (Carl Zeiss Microscopy GmbH, Jena, Germany) at an accelerating voltage of 10 kV.

Atomic Force Microscopy images were recorded to determine the micropattern thickness. The MFP-3D microscope (Asylum Research, Santa Barbara, CA) equipped with a Point probe NCL cantilever (Nanosensor, Wetzlar-Blankenfeld, Germany, k_c = 45 N m^{-1}, R = 25 nm) was used. The AFM heigh image of 50 μm^2 with a resolution of 256 × 256 pixels was recorded in tapping mode. The Gwyddion 2.53 software was used to determine the thickness profile, where the thickness would result as the average of three height measurements.

Atomic Force Microscopy-based Infrared Spectroscopy measurements on micropatterns were performed to collect chemical information of MIM

surfaces. IR spectra were recorded in the 900–1900 cm^{-1} range using a NanoIR2s (Bruker/Anasys Instruments) coupled to a multichip QCL source (MIRcat, Daylight Solutions; tuneable repetition rate range of 0–500 kHz;). An Au-coated silicon probe (PR-EX-nIR2 contact AFM-IR cantilever) with a spring constant of 0.07–0.4 nN m^{-1}, 30 nm tip radius and 75 kHz resonance frequency were used. AFM-IR spectra were obtained using 1024 co-averages for each data point with a spectral resolution of 2 cm^{-1}. The second contact mode was used to adjust the laser repetition rate. The presented spectra were an average of seven raw spectra with an adjacent averaging filter (5 pts) and a Savitzky-Golay filter (second older, 5 pts) applied.

Fluorescence array scanner (Genetic Microsystems GMS 418 Array Scanner) with 10 µm special resolution was used to detect DNA immobilization. Images were acquired with the Array Scanner software provided by GMS 418 with green and red lasers at excitation wavelengths of 532 and 635 nm, respectively. The green laser was set to 50 power and 50 gain by the software. For measurements with 635 nm excitation, the laser power was set to 100, and gains of 50 and 20 were used for PDA and MI-dPG, respectively. For concentration-dependent investigation of *poly*-A-Cy5 the laser power was set to 100 and the detector signal gain to five. Fluorescence intensities are values calculated by subtracting the averaged intensities of MI-dPG-*poly*-A from MI-dPG-*poly*-A-T-Cy5 recorded at 635 nm excitation.

Fluorescence microscopy Imaging was performed on a Leica SP8 equipped with a 100× oil immersion objective with a numerical aperture of 1.4 and a pE-4000 LED light source (CoolLED Ltd, Andover, UK). The fluorescence of the MI-dPG nanoarray was excited at 635 nm for 500 ms at 95% LED intensity. The pixel size of the recorded images was 41.4 nm. The obtained fluorescence images of MI-dPG-A25 before and after T25Cy5 hybridization (15 µl of 10 µM T25Cy5 for 30 min) were analyzed using ImageJ.[41] The intensity histograms of the images were adjusted to improve the visibility of the fluorescence signal. The autofluorescence of MI-dPG-*poly*-A was detected at 7.0 ± 0.5 RFU. For the image taken after *poly*-T-Cy5 hybridization, the signal threshold of 40–255 RFU and the fluorescence spot size of 0.45–0.65 μm^2 selection criteria were used to detect the fluorescence intensity of each spot of the nanoarray. The value and measurement error were calculated as the mean and standard deviation of all in-plane spots within the above analysis criteria.

Supporting Information

Supporting Information is available from the Wiley Online Library or from the author.

Acknowledgements

The authors thank Christiane Weimann for the assistance with SEM and EDX. IT acknowledges funding by the Deutsche Forschungsgemeinschaft (DFG, German Research Foundation) under grant number 457594480. MBH acknowledges funding by the Deutsche Forschungsgemeinschaft (DFG, German Research Foundation) under grant number 442240902 (HA 8528/2-1). The authors would also like to thank Core Facility BioSupraMol (Freie Universität Berlin, Germany) for the support in MIM synthesis.

Open access funding enabled and organized by Projekt DEAL.

Conflict of Interest

The authors declare no conflict of interest.

Data Availability Statement

The data that support the findings of this study are available from the corresponding author upon reasonable request.

Keywords

dendric polyglycerol, direct laser writing, micropatterning, mussel-inspired materials, polydopamine

Received: October 17, 2023
Published online: November 15, 2023

[1] M. Vaezi, H. Seitz, S. Yang, *Int J Adv Manuf Technol* **2013**, *67*, 1721.
[2] J. Stampfl, R. Liska, A. Ovsianikov, *Multiphoton Lithography: Techniques, Materials, and Applications*, Wiley, Weinheim, Germany **2017**.
[3] C. Greant, B. Van Durme, J. Van Hoorick, S. Van Vlierberghe, *Adv. Funct. Mater.* **2023**, *33*, 2212641.
[4] J. C. Williams, H. Chandrahalim, J. S. Suelzer, N. G. Usechak, *Adv. Photonics Res.* **2022**, *3*, 2100359.
[5] A. Braun, S. A. Maier, *ACS Sens.* **2016**, *1*, 1155.
[6] Q. Geng, D. Wang, P. Chen, S.-C. Chen, *Nat. Commun.* **2019**, *10*, 2179.
[7] A. Balena, M. Bianco, F. Pisanello, M. De Vittorio, *Adv. Funct. Mater.* **2023**, *33*, 2211773.
[8] P. Kord Forooshani, B. P. Lee, *J. Polym. Sci., Part A: Polym. Chem.* **2017**, *55*, 9.
[9] B. K. Ahn, *J. Am. Chem. Soc.* **2017**, *139*, 10166.
[10] Z. Wang, H.-C. Yang, F. He, S. Peng, Y. Li, L.u Shao, S. B. Darling, *Matter* **2019**, *1*, 115.
[11] T. G. Barclay, H. M. Hegab, S. R. Clarke, M. Ginic-Markovic, *Adv. Mater. Interfaces* **2017**, *4*, 1601192.
[12] M. Liu, G. Zeng, K. Wang, Q. Wan, L. Tao, X. Zhang, Y. Wei, *Nanoscale* **2016**, *8*, 16819.
[13] H. A. Lee, E. Park, H. Lee, *Adv. Mater.* **2020**, *32*, 1907505.
[14] Q. Wei, K. Achazi, H. Liebe, A. Schulz, P.-L. M. Noeske, I. Grunwald, R. Haag, *Angew. Chem., Int. Ed.* **2014**, *53*, 11650.
[15] M. Li, C. Schlaich, M. Willem Kulka, I. S. Donskyi, T. Schwerdtle, W. E. S. Unger, R. Haag, *J. Mater. Chem. B* **2019**, *7*, 3438.
[16] M. Czuban, M. W. Kulka, L. Wang, A. Koliszak, K. Achazi, C. Schlaich, I. S. Donskyi, M. Di Luca, J. M. Mejia Oneto, M. Royzen, R. Haag, A. Trampuz, *Mater. Sci. Eng. C Mater. Biol. Appl.* **2020**, *116*, 111109.
[17] Q. Wei, T. Becherer, P.-L. M. Noeske, I. Grunwald, R. Haag, *Adv. Mater.* **2014**, *26*, 2688.
[18] H. Lee, S. M. Dellatore, W. M. Miller, P. B. Messersmith, *Science* **2007**, *318*, 426.
[19] K. Sun, Y. Xie, D. Ye, Y. Zhao, Y. Cui, F. Long, W. Zhang, X. Jiang, *Langmuir* **2012**, *28*, 2131.
[20] H.-W. Chien, W.-H. Kuo, M.-J. Wang, S.-W. Tsai, W.-B. Tsai, *Langmuir* **2012**, *28*, 5775.
[21] Y. H. Ding, M. Floren, W. Tan, *Biosurf. Biotribol.* **2016**, *2*, 121.
[22] X. Du, L. Li, J. Li, C. Yang, N. Frenkel, A. Welle, S. Heissler, A. Nefedov, M. Grunze, P. A. Levkin, *Adv. Mater.* **2014**, *26*, 8029.
[23] I. Topolniak, A. M. Elert, X. Knigge, G. C. Ciftci, J. Radnik, H. Sturm, *Adv. Mater.* **2022**, *34*, 2109509.
[24] R. Batul, T. Tamanna, A. Khaliq, A. Yu, *Biomater. Sci.* **2017**, *5*, 1204.
[25] A. Dazzi, R. Prazeres, F. Glotin, J. M. Ortega, *Opt. Lett.* **2005**, *30*, 2388.
[26] R. A. Zangmeister, T. A. Morris, M. J. Tarlov, *Langmuir* **2013**, *29*, 8619.
[27] G. Sun, F. Zu, N. Koch, J. Rappich, K. Hinrichs, *Phys. Status Solidi B* **2019**, *256*, 1800308.
[28] Y. Ji, X. Yang, Z. Ji, L. Zhu, N. Ma, D. Chen, X. Jia, J. Tang, Y. Cao, A. C. S. Omega, *ACS Omega* **2020**, *5*, 8572.
[29] J. H. Ryu, P. B. Messersmith, H. Lee, *ACS Appl. Mater. Interfaces* **2018**, *10*, 7523.
[30] S. Chen, Q. Lu, *Adv. Healthcare Mater.* **2020**, *9*, 2001006.
[31] S. Fruncillo, X. Su, H. Liu, L. S. Wong, *ACS Sens.* **2021**, *6*, 2002.
[32] B. Derkus, *Biosens. Bioelectron.* **2016**, *79*, 901.
[33] K. T. M. Tran, T. D. Nguyen, *J. Sci.: Adv. Mater. Devices* **2017**, *2*, 1.

[34] R. J. Lipshutz, S. P. A. Fodor, T. R. Gingeras, D. J. Lockhart, *Nat. Genet.* **1999**, *21*, 20.
[35] Y. Kashima, Y. Sakamoto, K. Kaneko, M. Seki, Y. Suzuki, A. Suzuki, *Exp. Mol. Med.* **2020**, *52*, 1419.
[36] L. Cordsmeier, M. B. Hahn, *ChemBioChem* **2022**, *23*, 202200391.
[37] M. B. Hahn, *J Phys Commun* **2023**, *7*, 042001.
[38] M. B. Hahn, P. M. Dietrich, J. Radnik, *Commun Chem* **2021**, *4*, 50.
[39] D. S. Dandy, P. Wu, D. W. Grainger, *Proc. Natl. Acad. Sci. USA* **2007**, *104*, 8223.
[40] L. Yu, P. Tang, C. Nie, Y. Hou, R. Haag, *Adv. Healthcare Mater.* **2021**, *10*, 2002202.
[41] J. Schindelin, I. Arganda-Carreras, E. Frise, V. Kaynig, M. Longair, T. Pietzsch, S. Preibisch, C. Rueden, S. Saalfeld, B. Schmid, J.-Y. Tinevez, D. J. White, V. Hartenstein, K. Eliceiri, P. Tomancak, A. Cardona, *Nat. Methods* **2012**, *9*, 676.